Ultrasonics - Sonochemistry 44 (2018) 14–23

Contents lists available at ScienceDirect

Ultrasonics - Sonochemistry

journal homepage: www.elsevier.com/locate/ultson

Closed loop cavitation control – A step towards sonomechatronics

Kai-Alexander Saalbach*, Hendrik Ohrdes, Jens Twiefel

Institute of Dynamics and Vibration Research, Leibniz Universität Hannover, Hanover, Germany

ARTICLE INFO

Keywords:
Cavitation
Sonochemistry
Closed loop control
Closed loop cavitation control

ABSTRACT

In the field of sonochemistry, many processes are made possible by the generation of cavitation. This article is about closed loop control of ultrasound assisted processes with the aim of controlling the intensity of cavitation-based sonochemical processes. This is the basis for a new research field which the authors call “sonomechatronics”. In order to apply closed loop control, a so called self-sensing technique is applied, which uses the ultrasound transducer’s electrical signals to gain information about cavitation activity. Experiments are conducted to find out if this self-sensing technique is capable of determining the state and intensity of acoustic cavitation. A distinct frequency component in the transducer’s current signal is found to be a good indicator for the onset and termination of transient cavitation. Measurements show that, depending on the boundary conditions, the onset and termination of transient cavitation occur at different thresholds, with the onset occurring at a higher value in most cases. This known hysteresis effect offers the additional possibility of achieving an energetic optimization by controlling cavitation generation.

Using the cavitation indicator for the implementation of a double set point closed loop control, the mean driving current was reduced by approximately 15% compared to the value needed to exceed the transient cavitation threshold. The results presented show a great potential for the field of sonomechatronics. Nevertheless, further investigations are necessary in order to design application-specific sonomechatronic processes.

1. Introduction

Acoustic cavitation, that is the generation of cavitation by sound wave induced pressure changes, is used in many sonochemical processes like mixing or emulsification or for ultrasonic cleaning. Independent of its mechanism of generation, cavitation can be detected by vibrations (oscillation and implosion) caused by cavitation bubbles. Hydrodynamic cavitation in valves [1] or pumps [2] for example can be monitored observing the occurrence of certain frequency components. In acoustic cavitation, the generated frequency components are mostly related to the driving frequency f_0 of the ultrasound transducer [3–10]. Researchers [11–14] have shown that with a so called self-sensing technique, that is using the ultrasound transducer simultaneously as both an actuator and a sensor, indicators for the presence of cavitation can be detected by observing the transducer’s electrical signals. By now the transducer data [12,13] have been compared to those of microphones and hydrophones in order to reach a conclusion on the processes in the fluid. With this, the onset of cavitation and the transition between stable and transient or inertial cavitation could be detected but no quantification was possible.

In this contribution, a link is established between the cavitation activity determined from photographs and indicators in the transducer’s electrical data (self-sensing). This provides a new possibility for process monitoring. During the investigation of this monitoring technique, it was found that the hysteresis effect of cavitation [10,16–18] – mechanical amplitude can be reduced without affecting cavitation intensity after the threshold for inertial cavitation is exceeded – can also be monitored using self-sensing. The hysteresis effect offers an opportunity to energetically optimize acoustic cavitation generation. Because inertial cavitation is of a transient and chaotic nature, this process undergoes partly violent fluctuations. Therefore, an open loop process control is not sufficient for optimization. The design of a closed loop control is necessary.

Currently, several approaches to active closed loop cavitation control are known. For medical HIFU therapy by tissue heating [19–21] a feedback system has been designed. To monitor cavitation activity during tissue heating, a passive broadband single-element cavitation detector [22] is used as additional sensor. For the application of sonoporation several authors report closed loop concepts with hydrophone measurements to determine cavitation activity [23–26].

In Ref. [27] also a hydrophone is used to monitor acoustic emission of cavitation generated by a plane piezoelectric transducer for sonoporation. A closed loop is established to alter acoustic intensity based on acoustic emissions. These recent publications show that closed loop

* Corresponding author.
E-mail address: saalbach@ids.uni-hannover.de (K.-A. Saalbach).

https://doi.org/10.1016/j.ultsonch.2018.01.021
Received 6 July 2017; Received in revised form 30 November 2017; Accepted 26 January 2018
Available online 05 February 2018
1350-4177/

control of cavitation is a valuable target. Additional motivation to implement closed loop cavitation control are high power processes such as ultrasonic assisted hybrid casting [14], there cavitation is utilized to enable a pure metallic bond between aluminum melt and solid copper. The intensity of cavitation is crucial for the quality of the connection. Since the few known implementations of closed loop cavitation control are application focused a transfer to further processes is needed. This encourages to propose a general concept for process control of acoustic cavitation regardless if further sensors can be used or not.

In this contribution the concept of monitoring acoustic emissions for closed loop cavitation control is applied to an exemplary sonochemical power ultrasound process. Instead of using an additional sensor like a hydrophone, the self-sensing concept is implemented for detection of acoustic emissions. In order to be able to generate cavitation application-specific in this contribution, a double set point closed loop control [28] for controlling cavitation intensity for power ultrasonics is presented. As control parameter, an indicator in the ultrasound transducer's electrical signals is used, which makes the application of additional measuring equipment unnecessary. Next, the concept of sonomechatronics is described in detail. Subsequently, the principle of the applied self-sensing technique is explained, the experimental setup is described and the transducer's sensor characteristic is investigated. This is followed by the explanation of the possibility of energetic optimizability and finally the implemented closed loop control is presented.

2. Introducing the concept of sonomechatronics

The concept of sonomechatronics is based on a classic mechatronic concept, where mechanics, electronics and information technology are combined in one system. For a sonomechatronic system, the classic mechatronic concept is expanded and includes the chemical domain, see Fig. 1. The combination of mechanics, or in this case acoustics, and chemistry is well known as sonochemistry. The sonomechatronic concept then combines sonochemistry with electronics and information techniques which makes it possible to observe and control sonochemical processes. Most sonochemical processes are not controlled by means of the sonochemical results. For example, the process time or energy are based on experience values. For this reason, it is most probable that the process is unnecessarily long or the energy input is

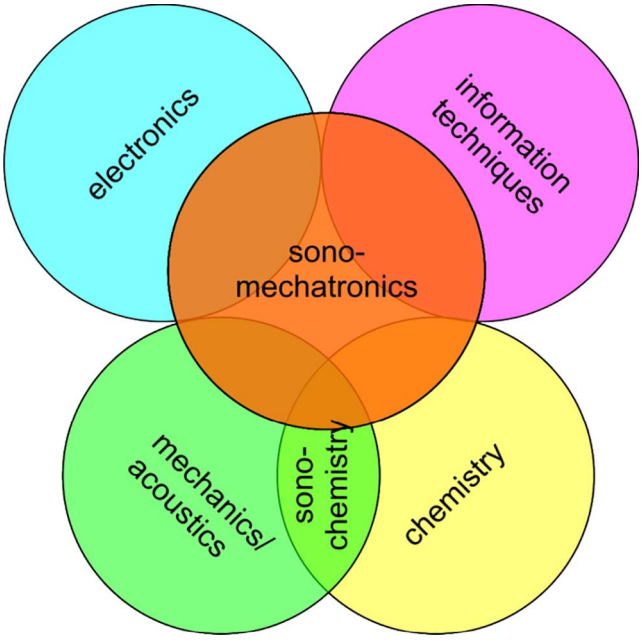

Fig. 1. Concept of sonomechatronics – different disciplines.

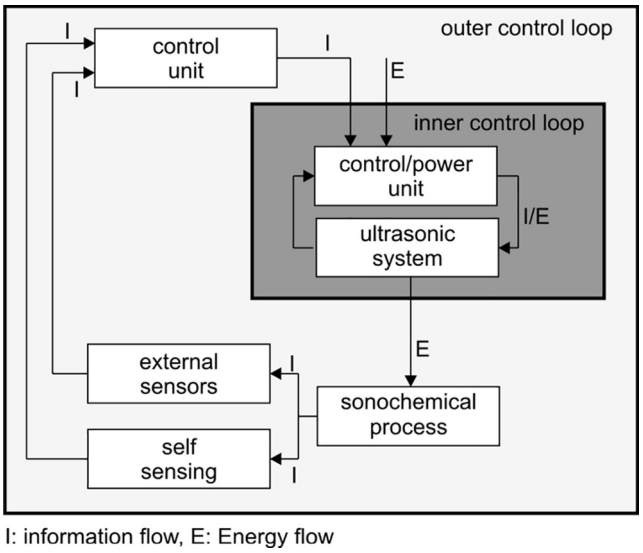

Fig. 2. Inner and outer control loop in sonomechatronical applications.

higher than necessary to guarantee a completed sonochemical process. This directly leads to a waste of energy. To overcome this issue, sonochemical processes can be sensed and the sensor data can be used to adapt the ultrasonic system. With this attempt, the transducer can be driven in an operation condition that fits the sonochemical process and stops when the desired processing result is reached. This approach can be reached using two control loops, see Fig. 2. The inner control loop controls the ultrasonic system to drive it in resonance at desired amplitude.

In order to bring the system in an optimal operation condition for the process, the outer control loop uses the sensor data or self-sensing data to adapt, for example, the desired driving amplitude or power for the inner control unit. The system will be turned off as soon as the desired result is reached and sensed, thus the issue of overprocessing is solved.

3. Principle of self-sensing cavitation detection

For clarification before the experimental setup is described and the results are presented, the principle of self-sensing cavitation detection is now explained in more detail.

The bolt clamped piezoelectric power ultrasound transducer [29], used for this investigation, consists of three different parts. A converter, a booster and a Sonotrode, which is in contact with the process medium. The transducer used for this investigation is an experimental transducer manufactured at Institute of Dynamics and Vibration Research driven at its third longitudinal eigenmode at a frequency of approximately 20 kHz. Driving the transducer in resonance has the benefit that the phase value between the electrical current and voltage at the transducer's terminals is 0°, which corresponds to a purely resistive behavior. For the transducer used in the experiments, as typical for ultrasound transducers driven at resonance, at this driving point the relationship between electrical current and displacement amplitude is linearly proportional. A sketch and a photo of the mounted transducer are shown in Fig. 3.

By applying voltage to the piezoelectric ceramics, the converter is mechanically excited by the inverse piezoelectric effect. The vibration is transferred to the tip of the sonotrode via the geometry. The transducer's transfer function changes when a load is applied to the tip of the sonotrode. These changes include, for example, a shift in resonance frequency, f_0, and the electrical admittance, Y_{el}. The basis of self-sensing cavitation detection is the fact that the converter is able to convert electrical signals in mechanical vibration and vice versa. When

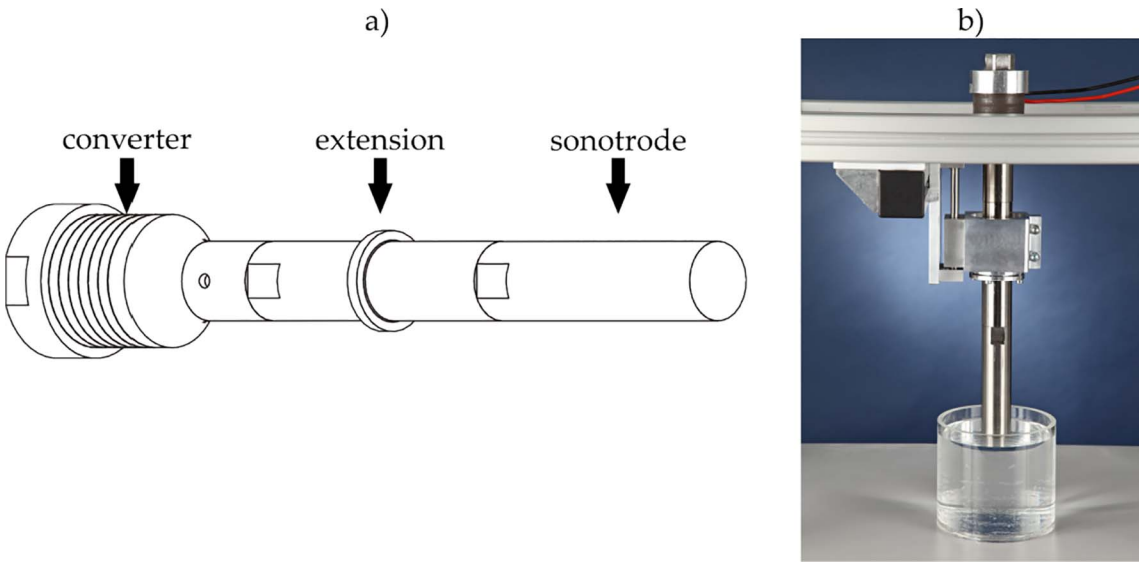

Fig. 3. Piezoelectric ultrasound transducer used for experiments: a) sketch of ultrasound transducer, b) mounted transducer with tip of sonotrode immersed in water.

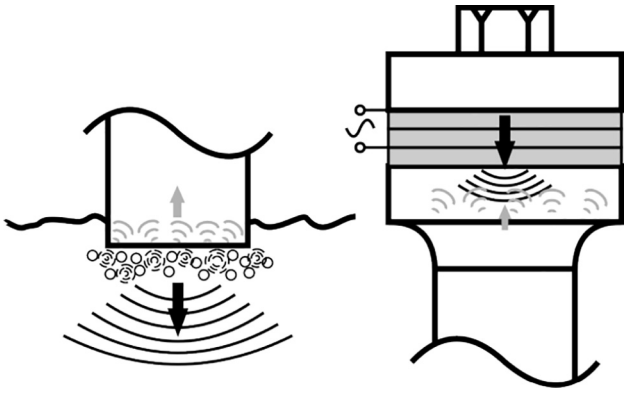

Fig. 4. Principle of self-sensing cavitation detection: Vibration due to driving signal shown in black, vibration due to cavitation reaction shown in gray.

cavitation is generated, the oscillations and implosions of the bubbles cause pressure changes which excite and deform the tip of the sonotrode. These deformations are transferred to the piezoelectric ceramics via the geometry and generate electric signals through the piezoelectric effect. The signals caused by cavitation and the driving signal can be measured at the transducer's electrical terminals. Because the cavitation induced signals are small compared to the driving signal, they can hardly be recognized in the time domain. By transferring the signals at the terminals into the frequency domain, the different frequency components become visible. In addition to the bubble vibrations, cavitation also changes the composition of the fluid. Instead of pure liquid, a mixture of liquid and bubbles (gas) is present at the tip of the sonotrode. Changes in the transducer's characteristic caused by load changes at the tip of the sonotrode can also be observed at the transducer's terminals. The principle of self-sensing cavitation detection is shown in Fig. 4.

4. Experimental setup

For these investigations, the ultrasound transducer was used to generate a sound-field and create cavitation in water. Therefore, the sonotrode's tip was immersed in water within a cylindrical container made of polymethyl methacrylate (PMMA). This setup was already shown in Fig. 3b). In order to characterize the ultrasound transducer, its frequency response and the linear displacement-current characteristic in resonance were measured. The former was measured using the control hardware DPC500/100k [30] as a generator and connecting it to a power amplifier (QSC Audio RMX 4050HD). The transducer was connected to the amplifier and the voltage and current were measured at the electrical terminals of the transducer with a current and voltage probe while a frequency sweep was performed. The result of this measurement for the unloaded transducer is shown in Fig. 5a). Here the Admittance $|Y_{el}|$ and phase between current and voltage are shown for a frequency range around the frequency of the eigenmode used for driving. The measured relationship between displacement and current amplitude is shown in Fig. 5b). This measurement was performed using a laser vibrometer (Polytec OFV-552 and vibrometer controller OFV-5000) and by measuring the displacement in the middle of the sonotrode's front face. For this measurement, the current amplitude was increased in 100 mA increments from 100 to 2000 mA. The control hardware has two separate built-in PID-controllers for phase and current control. These were used to keep the current amplitude at the desired level and ensured that the transducer was driven in resonance at 0° phase at all times.

As a result, the linear relationship of 2.7 µm/A was determined in the measured range. Another feature of the control hardware is the compensation [31] of the transducer's parallel capacitance *Cp*. This allows for operation at resonance, even if a load changes the electrical characteristics so much that the electrical resonance frequency can no longer be identified by a phase value of 0°. The control hardware uses the parallel capacitance *Cp* of the Piezo ceramics to calculate the mechanical characteristic in which a phase value of 0° is always present. Hereby the resonance frequency can still be identified and controlled, even under heavy load.

For the presented investigations, a photo camera (Nikon D3100 + Sigma DC 18–250 mm lense), a hydrophone with preamplifier (Reson TC4034-1 with EC6061 voltage preamplifier VP1000), and a digital oscilloscope (Picoscope5203) were used. The hydrophone's transfer characteristic provided by the manufacturer and the transducer's calculated frequency response are shown in Fig. 6. The hydrophone's transfer characteristic shows sufficient uniformity up to 200 kHz. For higher frequencies the transfer characteristic shows an amplification with a maximum around approximately 320 kHz and high attenuation for frequencies higher than 400 kHz. The transducer's frequency response was calculated up to the forth harmonic of the driving frequency using a finite element model. In a harmonic response calculation, a force with the magnitude of 1 N was applied to the front face of the Sonotrode. As a reaction to the applied force the charge at the terminals of the piezo elements was computed which was then used to

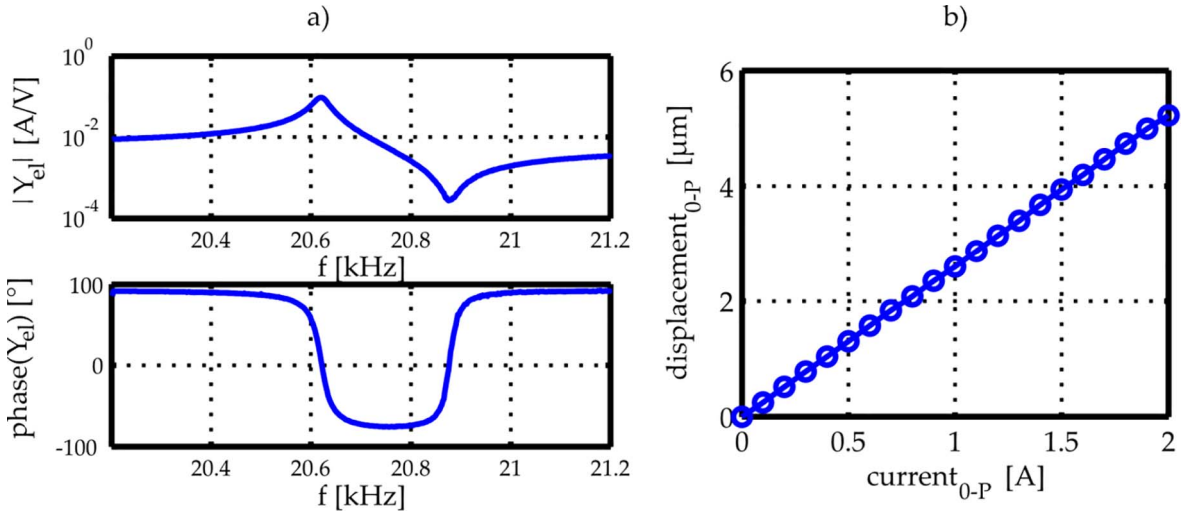

Fig. 5. Characteristics of the unloaded transducer: a) admittance $|Y_{el}|$ and phase measured around the resonance frequency used for driving, b) transducer's measured displacement – current characteristic.

compute the generated current. As can be seen in Fig. 6b), the transducer shows high sensitivity at several distinct frequencies.

The tip of the sonotrode was immersed at different depths in water in the center of the water container. The tip of the hydrophone was also immersed in water, approximately in the middle between the sonotrode and the edge of the water container. The oscilloscope was used to ascertain the transducer's electrical data and the hydrophone signal. It was also used to trigger the camera. With a measurement software programmed in Labview, data blocks of 20,000 samples were recorded at a sampling rate of 1 Msamples/s. A photo was also taken for each datablock. The camera was placed in front of the water container and photos were taken to determine the amount of cavitation inside the container. Lighting was aligned in a way that the light fell through the container towards the camera. Bubbles inside the liquid then could be detected by changes in brightness. In order to determine the bubble content, a reference photo was taken at the beginning of every measurement and was later subtracted from the other photos. The number of changed pixels was determined through additional image processing. It is assumed that the number of changed pixels corresponds to the amount of cavitation generated. The pictures taken show only a part of the actual bubble content, which is due to the fact that the pictures only show a plane of a three-dimensional volume. The data obtained from the photographs are nevertheless assumed to be representative.

5. Transducer's sensor characteristic

In order to be able to use the transducer as a cavitation sensor, it is necessary to investigate which frequency components are generated with the experimental setup. Therefore, the signals recorded with the hydrophone are compared to the cavitation activity before a link is established between cavitation events and indicators in the transducer's current signal.

For a distance of 80 mm, the container is filled with water so that the tip of the sonotrode is immersed at a depth of 2 mm. From this position, for subsequent measurements the sonotrode is lowered to adjust 75 mm, 70 mm and 65 mm distance between the tip of the sonotrode and the bottom of the water container. The driving current amplitude is increased stepwise for the measurements.

Fig. 7 shows the results of a measurement for a distance of 75 mm. In Fig. 7a) the increasing excitation during the experiment is shown. This was similar for all measurements. The control hardware keeps the current amplitude at the set point value with minor deviations for up to about 70 s. From this point on the controller action becomes stronger.

Fig. 7b) shows the evaluation of the photos taken during the experiments. The number of black pixels after image processing, which correspond to the amount of cavitation, is shown. Since the cavitation bubbles are of different sizes, the photos contain a different number of pixels for the individual bubbles. Additionally, the photo studies used are affected by errors, since the change in the individual images with respect to a reference photo has been evaluated. In this way, for

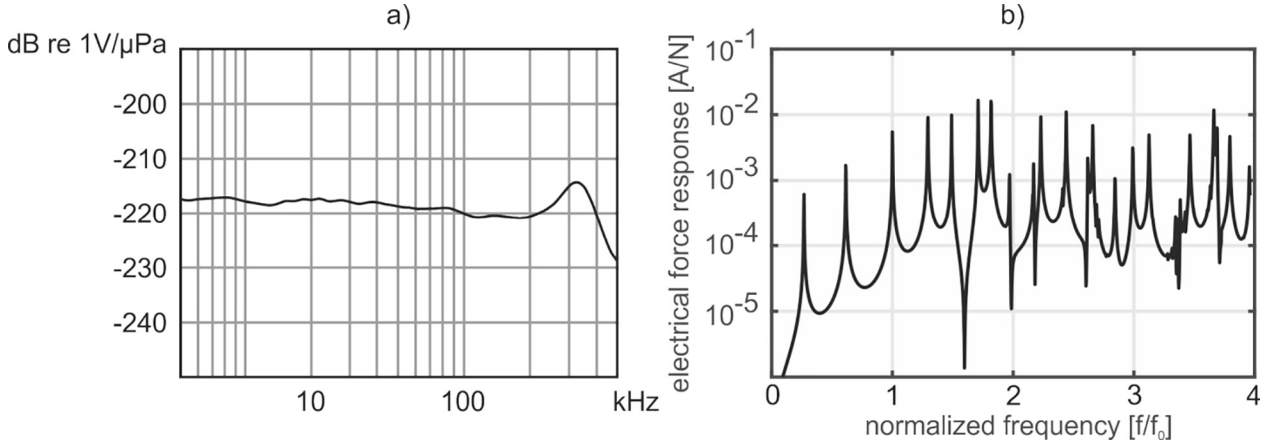

Fig. 6. Frequency response: a) hydrophone (measured by manufacturer), b) ultrasound transducer (from finite element calculation).

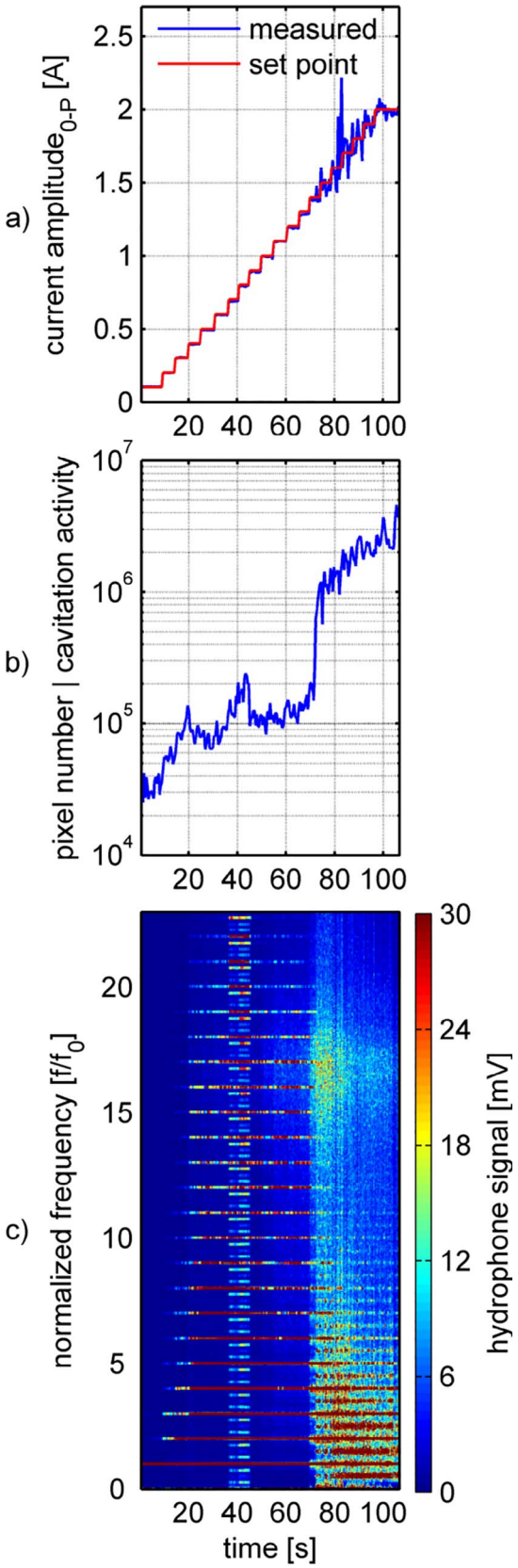

Fig. 7. Cavitation activity and frequency spectrum generated during increasing excitation: a) excitation (set point value and measured current), b) number of black pixels corresponding to cavitation activity, c) spectrogram of hydrophone measurement.

example, movement of the water surface and bubbles which attach to the vessel wall are evaluated as cavitation activity. Furthermore, the photos do not show the complete contents of the container, since they are a snapshot from one side of the container. Nevertheless, the evaluation of the photographs gives a quantification of the cavitation activity to establish a connection with generated frequency components. For the evaluation, the total number of pixels allocated to the cavitation bubbles is used for each photo to obtain a measure for the cavitation activity. The starting value exists due to gas bubbles, which are dissolved in the liquid and begin to vibrate once the ultrasound is switched on. The decrease of the amount of cavitation in the first seconds is most likely due to degassing of the liquid at low excitation amplitudes. After approximately 10 s, the cavitation intensity increases due to increasing excitation. Fig. 7c) shows the corresponding spectrogram of the hydrophone measurement. At this point in the measurement the 2nd and 3rd harmonic appear. At 20 s a peak in the cavitation activity is visible. This is accompanied with the onset of multiple harmonics in the spectrogram of the hydrophone signal. This indicates that the threshold for stable cavitation has been exceeded. Another peak in cavitation activity appears for a short time at approximately 40 s. For this time point, in addition to the harmonics already present, the spectrogram shows the subharmonics $1/4f_0$ and $3/4f_0$ and multiple ultraharmonics $n + 1/4f_0$ and $n + 3/4f_0$, with n being the harmonic index (n = 2, 3, …). By evaluating the photographs, the occurrence of these frequency portions can be linked with the appearance of a jelly-fish streamer [15].

The cavitation activity increases by factor 8 to approximately 1.2×10^6 at approximately 70 s. Here the excitation amplitude is increased to 1.4 A, which seems to generate a pressure high enough to trigger transient cavitation. This is linked to the onset of broad band noise in the spectrogram and increased amplitudes of ultraharmonics ($n/2f_0$) in the lower frequency range up to the 9th harmonic. Additionally, a broad noise band between the 14th and 19th harmonic appears in the spectrogram. This indicates that the threshold for inertial cavitation has been exceeded. The appearance of the noise band between the 14th and 19th harmonic is very likely caused by amplification due to the hydrophone's transfer characteristic (Fig. 6), which shows a higher sensitivity in this frequency range than at lower frequencies. The photographs show large cavitation zones appearing and moving throughout the container. The level of this noise band decreases after approximately 10 s and the ultraharmonic content in the region below the 7th harmonic increases. The chaotic generation of bubbles and the related changes in the mixture of gas and fluid cause rapid changes in acoustic impedance. This changes the load at the tip of the sonotrode and leads to stronger controller action. The connections between the cavitation intensity, the indicators in the hydrophone signal and the activity of the amplitude controller are the same for the remaining immersion depths.

Now that the cavitation events are linked to indicators in the hydrophone signal, the sensor properties of the ultrasound transducer are investigated. Fig. 8b) shows the spectrogram of the transducer's current signal corresponding to the experimental data shown in Fig. 7. Since the transducer is primarily used as an actor for the generation of cavitation, it is necessary to find out which frequency fractions are present in the current signal due to the operation as an actor without the reaction of cavitation. In order to do this, the transducer is driven without a load in air with the same stepped excitation as shown in Fig. 7a). The spectrogram for this unloaded operation is shown in Fig. 8a). It can be seen that, with increasing excitation amplitude, harmonics of the driving frequency are generated.

Ultraharmonics ($n/2f_0$) are especially present above the 5th harmonic. In addition, the global noise level increases. These generated frequency components are known as acoustic cavitation indicators for stable and transient cavitation and could already be used to establish a connection between the cavitation activity and the hydrophone signal. Due to the presence of frequency portions, which are known as indicators for cavitation, in the current signal, even without a load, the

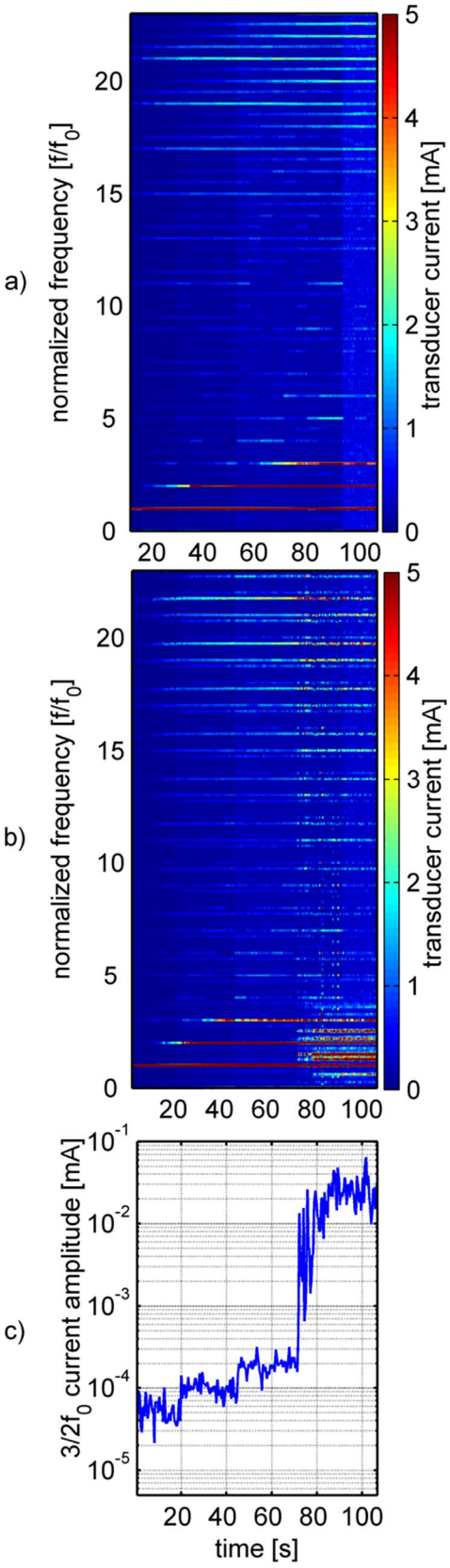

Fig. 8. Ultrasound transducer's sensor characteristic: a) spectrogram of current signal of unloaded transducer with stepped excitation as in Fig. 7 a), b) spectrogram of current signal during experiment shown in Fig. 7, c) mean value of $3/2f_0$ in transducer current signal during experiment shown in Fig. 7.

occurrence of harmonics and an increasing noise level cannot be used as cavitation indicators with the self-sensing technique without further examination. Since the sensitivity of the transducer, as shown in Fig. 6b), is high at the harmonics and some ultra-harmonic frequencies, it can be assumed that these frequency components cannot be used as indicators of cavitation activity.

One major change occurring in the spectrogram of the current signal when cavitation is generated is the presence of subharmonic and ultraharmonic content below the 4th harmonic from the moment inertial cavitation occurs. With the onset of inertial cavitation, several distinct frequencies become visible, namely $5/4f_0$, $3/2f_0$, $7/4f_0$, $15/7f_0$ and $5/2f_0$. Here a change occurs when the level of the noise band between the 14th and 19th harmonic in the hydrophone measurement decreases and energy is transferred to the frequency range below the 7th harmonic. In the current signal, additional subharmonic content $0.26f_0$ and $3/5f_0$ appears. With the onset of the subharmonic content, the level of the ultraharmonics already present increases.

The broad band noise generated by transient cavitation, which could be detected with the hydrophone, is strongly altered in the current signal by the transfer characteristic of the ultrasound transducer. The transducer's high sensitivity towards distinct ultraharmonic frequency portions limits the usable frequency range for cavitation detection. This leads to the occurrence of ultraharmonic content in the current spectrogram when transient cavitation is generated.

The analysis of the transducer's current signal shows that the onset of stable cavitation cannot be detected by the onset of harmonics of the driving frequency. These frequency portions are already generated by the transducer due to its excitation. The onset of inertial cavitation can be detected by generation of ultraharmonics below the 4th harmonic. One frequency component from this range, which shows good correspondence with the cavitation activity is the $3/2f_0$ frequency portion. Fig. 8c) shows the evaluation of the amplitude of this portion from the transducer's current signal. While the cavitation activity in Fig. 7b) increases by factor 8 due to the onset of inertial cavitation, the amplitude of the $3/2f_0$ portion also increases but by factor 86.

The presented procedure for identification of usable cavitation indicators for self-sensing now easily can be applied to arbitrary cavitation processes. This includes the following steps: determination of the transducer's transfer characteristic, identification of frequency ranges excited directly by the power electronics, recording the electrical signals during operation, analysis of the generated frequency content, identification of potential indicators by comparison of the frequency content in loaded and unloaded state, and proof of indicators using a reference measurement.

This procedure is suitable for different operation modes such as continuous driving (used in the example), amplitude modulation or frequency modulation. However, the impact of the driving mode on the electrical signals has to be considered in the indicator selection.

6. Energetic optimizability

In order to study the relationship between the amount of cavitation and the $3/2f_0$ portion in more detail, further experiments were conducted in which the excitation amplitude was increased and then decreased again. For these experiments, the hydrophone was removed and the excitation amplitude was increased and decreased in 50 mA increments. The maximum value was 1.5 A. Apart from this, the experimental procedure was not altered. The investigations showed that the hysteresis effect leads to different thresholds for the onset and termination of inertial cavitation, as can be seen in Fig. 9a). For a distance of 80 mm between the container bottom and the tip of the sonotrode, the course of the $3/2f_0$ frequency portion is shown during stepped in- and decrease of excitation amplitude. When excitation is increased, the $3/2f_0$ portion increases sharply when 1150 mA is reached. This indicates that the threshold for inertial cavitation has been exceeded. When reducing excitation amplitude again, the $3/2f_0$ portion decreases sharply

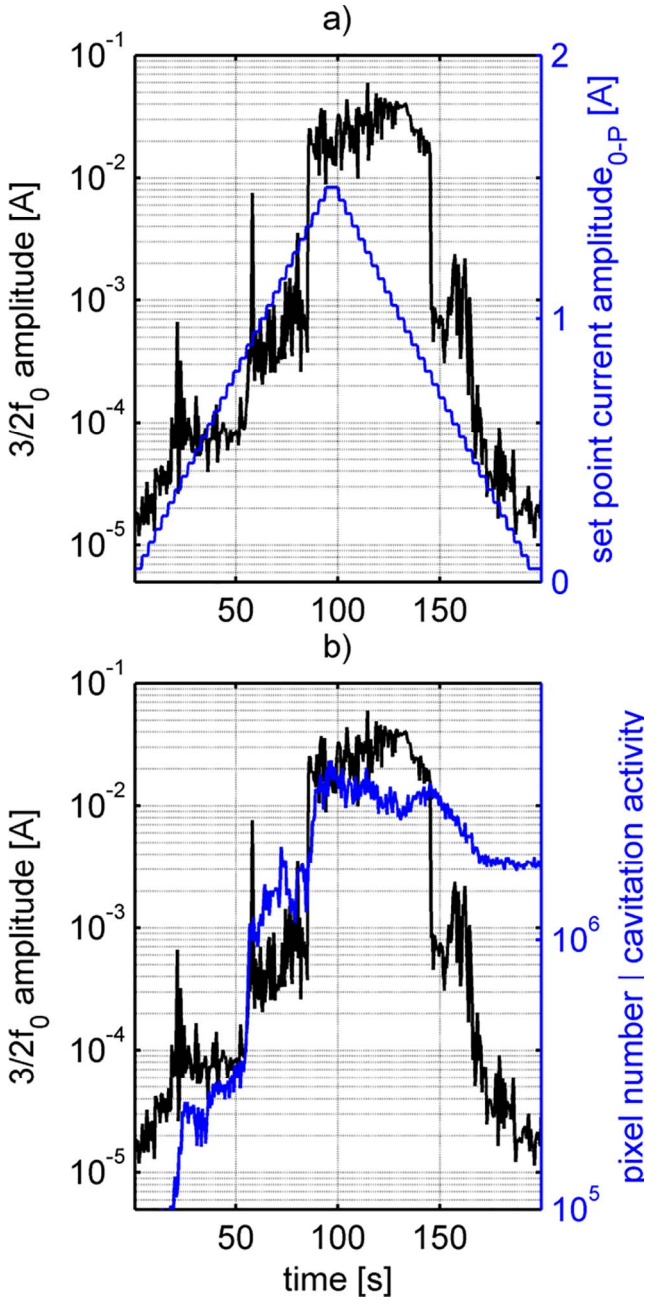

Fig. 9. Connection between $3/2f_0$ frequency portion and cavitation activity for 75 mm: a) stepping the excitation amplitude up and down the $3/2f_0$ portion decreases at lower amplitude than it increases, b) cavitation activity and $3/2f_0$ portion increase at the same time.

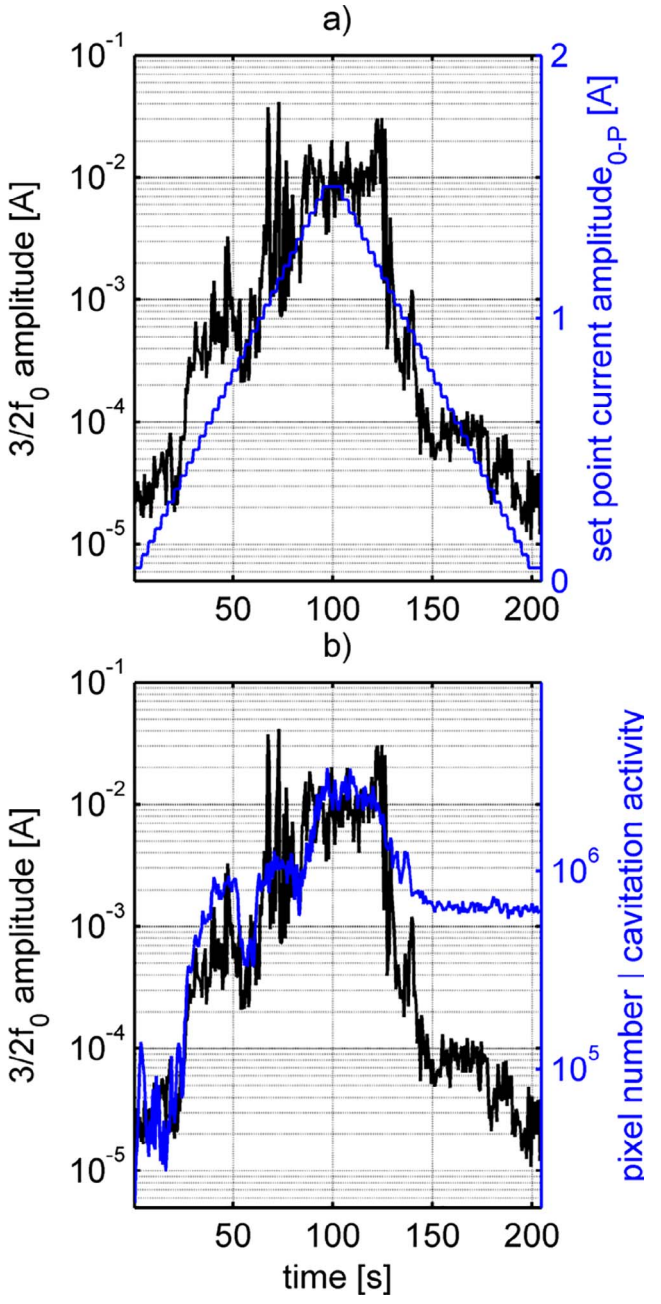

Fig. 10. Connection between $3/2f_0$ frequency portion and cavitation activity for 65 mm: a) excitation amplitude and $3/2f_0$ portion, b) cavitation activity and $3/2f_0$ portion increase at the same time.

when the driving current is reduced to less than 850 mA. Now inertial cavitation is terminated again. This hysteresis effect has been reported by several researchers [10,16–18]. The two different thresholds for the onset and termination of inertial cavitation show a potential for energetic optimization. Once the threshold for inertial cavitation has been exceeded, the excitation amplitude can be reduced while the state of inertial cavitation is still maintained. The suitability of the $3/2f_0$ frequency portion as an indicator for the onset and termination of inertial cavitation is once more shown in Fig. 9b). Here the cavitation activity determined by photographs is shown together with the $3/2f_0$ frequency portion for the stepped increase and decrease of excitation amplitude. Both cavitation activity and $3/2f_0$ portion increase sharply when the current amplitude reaches 1150 mA. In contrast to the frequency indicator, the cavitation activity does not decrease sharply again when the current amplitude is decreased below 850 mA. The cavitation activity maintains a high value due to bubbles sticking to the wall of the water container. These bubbles are left from previous cavitation activity and represent an offset for subsequent values.

The difference between the onset and termination threshold differs with varying boundary conditions, i.e. immersion depths. Furthermore, the value the cavitation indicator reaches is different for different boundary conditions. Precise knowledge of the characteristics of the experimental setup is therefore essential. Fig. 10 shows the hysteresis effect and the connection between the $3/2f_0$ frequency component and the cavitation activity for a distance of 65 mm. From the spectrograms (not shown here) it is found that transient cavitation occurs between 85 and 125 s. In this timespan the cavitation indicator shows values around 0.01 A (Fig. 10a)). During the increasing phase the indicator reaches this value after 1.4 A is exceeded. During decreasing phase the driving

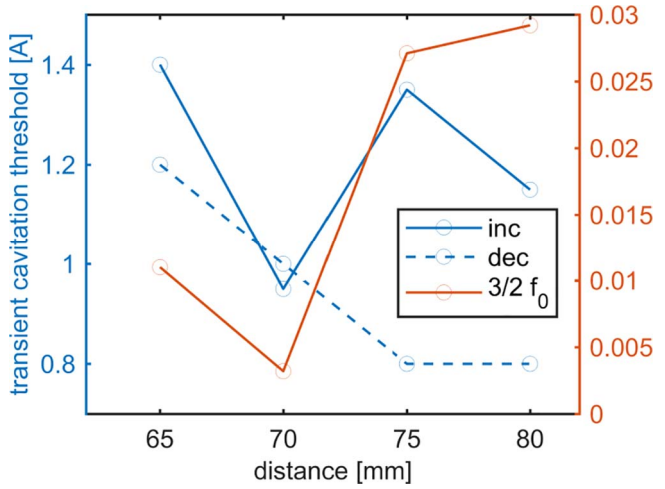

Fig. 11. Evaluation of the transient cavitation thresholds and the mean value of the cavitation indicator for all distances investigated.

current can be decreased to 1.2 A before the cavitation indicator falls to lower values. From Fig. 10b) again it can be seen that the $3/2f_0$ component shows good agreement with the cavitation activity.

The dependence of the transient cavitation thresholds and the mean value of the cavitation indicator on immersion depth are evaluated next. The result is shown in Fig. 11. From the differences between the cavitation thresholds for increasing and decreasing driving current the different magnitudes of the hysteresis effect become apparent. The results show that the amplitude can be reduced at 80 mm, 75 mm and 65 mm distance to still maintain transient cavitation. But for 70 mm distance there is a negative hysteresis, which means that the cavitation threshold is lower for increasing excitation. This difference can be partly explained with the formation of a standing wave between sonotrode's tip and vessel bottom. If the distance is near the wavelength of a standing wave the energy needed for the generation of cavitation is lower than for non-resonant configurations. If, on the other hand, the distance is chosen so that the sonotrode's tip is located near a node of a standing wave, the generation of cavitation consumes more energy. The wavelength of a standing wave can be computed by dividing the speed of sound in the liquid c_{H2O} by the driving frequency f_0 of the transducer. Although it is easy to determine the driving frequency of the transducer from the recorded data, the determination of the speed of sound of the two-phase fluid during cavitation generation is a challenge that cannot be readily done. On the basis of the speed of sound of pure water at room temperature, however, a rough estimate of the approximate wavelength λ can be performed. Assuming that the speed of sound is $c_{H2O} = 1500$ m/s and the transducer is driven at approximately 20.6 kHz, the approximate wavelength is 72 mm. Changes in driving frequency, which occur during cavitation generation, and an altered speed of sound of course change this value.

The explanation for the differences in cavitation threshold that results from the standing wave theory is as follows: A distance of 70 mm is nearly the wavelength of a standing wave. Therefore the threshold for cavitation generation during increasing phase is the lowest. By changing the distance, the resonance condition is violated and more energy is required for the generation of cavitation, which leads to higher cavitation thresholds. However, the threshold value for 80 mm is lower than for 75 mm. Further the threshold for decreasing excitation shows a different course than for increasing amplitude. Even though these two circumstances show that the explanation is not sufficient for a full understanding, it gives a good approximation.

In addition to the cavitation thresholds the mean values of the $3/2f_0$ cavitation indicator during transient cavitation are shown in Fig. 11. The mean values are computed for the individual timespan for that transient cavitation was generated. The qualitative course is similar to that of the cavitation thresholds for increasing excitation. The results show that the values vary and the value of the indicator has to be determined for the individual case. However, a measurement for the determination of this value is not complex.

7. Closed loop control

An efficient way to exploit the threshold difference in order to minimize the energy required during cavitation generation is the implementation of a closed control loop, which regulates the excitation current as a function of cavitation intensity. In the next step, such a closed loop control was set up using the $3/2f_0$ frequency portion in the transducer's current signal as an indicator for inertial cavitation and cavitation activity.

The control loop was setup in a cascaded manner, so that the cavitation intensity controller was used to set the control hardware's current amplitude set point value. For every dataset acquired, a FFT was calculated and the peak value for the $3/2f_0$ portion m_{32} was determined. This value was subtracted from the $3/2f_0$ set point value sp_{32}. Then the error $e_{32} = sp_{32}\text{-}m_{32}$ was calculated. Since the control loop was implemented in Labview the controller frequency is dependent on the overall system performance of the used computer. Therefore, a specification in terms of iterations is made rather than in seconds. For this investigation the controller changed the set point value after every iteration of the Labview program with a constant value of 10 mA for increase and decrease.

Depending on the value of e_{32}, the current amplitudes set point value was increased or decreased. Also, a range for e_{32} for which the cavitation controller would not perform any action could be defined. A sketch of the closed control loop is shown in Fig. 12.

As shown in chapter 6, the challenge in controlling cavitation processes is the sudden increase in cavitation activity, which is accompanied by the sudden increase of the cavitation indicator. Therefore, only certain values of the cavitation indicator can be used as set point values. The dependence on the boundary conditions has already been mentioned.

Fig. 13 shows the measured current amplitude during operation with active closed loop cavitation control. The set point value for the $3/2f_0$ cavitation indicator was set to 0.01 A and the distance between container bottom and sonotrode tip was 65 mm.

From the starting value, which was set to 100 mA, the current amplitude is increased until it reaches approximately 1.5 A (Fig. 13a)). For this excitation amplitude, the threshold for inertial cavitation is exceeded. This is indicated by the value of the $3/2f_0$ frequency component which jumps to a value around 0.01 A. Because of the chaotic and transient nature of cavitation the controller is changing the current set point value continually and the value of the cavitation indicator varies in a wide range between 0.001 A and 0.08 A. An inertial cavitation state is maintained for the rest of the operation. The transducer's current amplitude is constantly altered, which leads to a mean current amplitude value of 1.28 A. Compared to the threshold value of 1.5 A needed to generate inertial cavitation in the first place, the mean current amplitude was reduced by approximately 15%.

8. Conclusion and discussion

This article presents the novel field of sonomechatronics and provides a definition for it. The sonomechatronic application presented here deals with closed loop control of transient cavitation processes. An innovative approach for the detection of cavitation intensity is used for this purpose. After the concept of the applied self-sensing technique was explained, the performance of this technique was tested. Using a hydrophone as a reference sensor, a connection between the occurrence of several frequency based cavitation indicators and cavitation activity inside the fluid was made. The study of the ultrasonic transducer used showed that only some of these indicators can be used in the self-

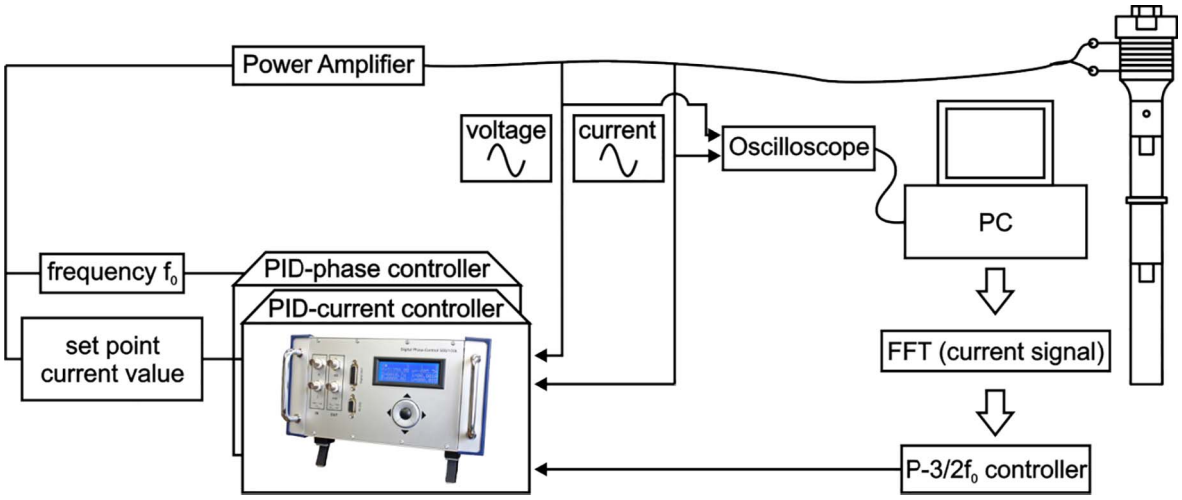

Fig. 12. Sketch of closed control loop.

sensing technique, since harmonics of the driving frequency and broadband noise already occur in the unloaded operation of the transducer. It was found that for the onset of inertial cavitation the 3/$2f_0$ frequency component can be used as an indicator. This indicator showed good correspondence with the cavitation activity. The cavitation hysteresis effect was also found in this investigation. Once the threshold for inertial cavitation was exceeded, the excitation amplitude could be reduced to still maintain inertial cavitation. This was utilized to implement a closed control loop, which controlled cavitation intensity by observing the previously identified cavitation indicator with the self-sensing technique. It was shown that driving the transducer with this control can reduce the mean current amplitude and therefore reduce energy consumption. The possible reduction is dependent on boundary conditions e.g. immersion depth which also influences the attenuation of the sonotrode.

Even though the results shown here are only valid for the experimental setup used, the outcomes present that a transfer of the concept to many sonochemical applications is very promising. This will allow the control of cavitation intensity which is helpful for general process control. Resulting effects such as increased efficiency depend on individual configuration properties of the components and medium.

The different thresholds for the onset and termination of inertial cavitation strongly depend on boundary conditions, including immersion depth, as well as fluid characteristics. As bubble movement is affected by the viscosity of the fluid, a change in viscosity will affect the emitted frequency spectrum and hence the self-sensing capability. Also the thresholds for generation of transient cavitation will vary with viscosity. Furthermore, the current amplitudes for the onset and termination of inertial cavitation depend on the transducer's current-displacement characteristic.

For the control of cavitation intensity, it is necessary to know the threshold value reached by the cavitation indicator for inertial cavitation. This also depends on the boundary conditions. The cavitation intensity controller used was a rudimentary controller implemented for test purpose. For optimal control, a more complex control strategy should be used, e.g. a PID-controller. However, the difficulty remains that, due to its jump behavior, the cavitation indicator only shows certain values.

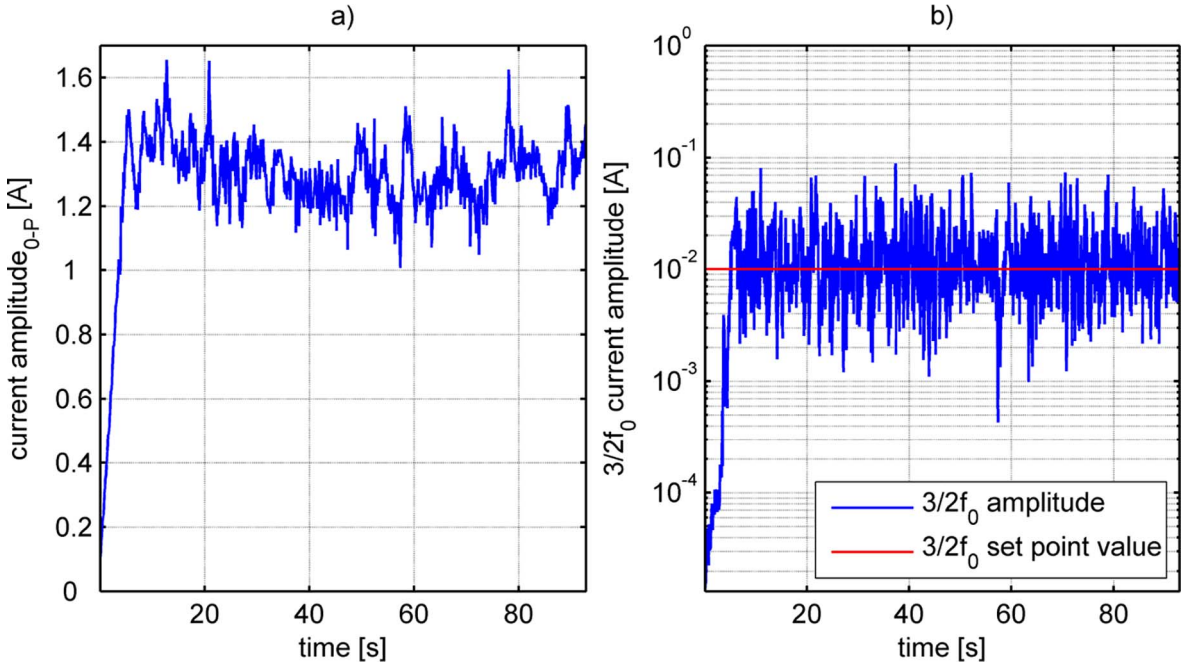

Fig. 13. Closed loop controlled cavitation generation at 65 mm distance: a) current amplitude during controlled operation, b) 3/$2f_0$ frequency component during controlled operation.

The investigations show a great potential for the field of sonomechatronics and the optimization of cavitation processes. Currently, the detection of cavitation intensity depends on the ultrasound system used and how the feedback controller design can be improved. Therefore, further investigations are necessary in order to be able to design application-specific sonomechatronic processes.

References

[1] B.-S. Yang, W.-W. Hwang, M.-H. Ko, S.-J. Lee, Cavitation detection of butterfly valve using support vector machines, J. Sound Vib. 287 (1) (2005) 25–43.
[2] M. CDdina, Detection of cavitation phenomenon in a centrifugal pump using audible sound, Mech. Syst. Signal Process. 17 (6) (2003) 1335–1347.
[3] E. Cramer, W. Lauterborn, Acoustic cavitation noise spectra, Appl. Sci. Res. 38 (1) (1982) 209–214.
[4] E.A. Neppiras, Measurements in liquids at medium and high ultrasonic intensities, Ultrasonics 3 (1) (1965) 9–17.
[5] E.A. Neppiras, Acoustic cavitation, Phys. Rep. 61 (3) (1980) 159–251 ISSN 0370–1573.
[6] E.A. Neppiras, Acoustic cavitation thresholds and cyclic processes, Ultrasonics 18 (5) (1980) 201–209 ISSN 0041–624X.
[7] M. Ashokkumar, M. Hodnett, B. Zeqiri, F. Grieser, G.J. Price, Acoustic emission spectra from 515 kHz cavitation in aqueous solutions containing surface-active solutes, J. Am. Chem. Soc. 129 (8) (2007) 2250–2258.
[8] P. De Santis, D. Sette, F. Wanderlingh, Cavitation detection: the use of the subharmonics, J. Acoust. Soc. Am. 42 (2) (1967) 514–516.
[9] P.W. Vaughan, Investigation of acoustic cavitation thresholds by observation of the first subharmonic, J. Sound Vib. 7 (2) (1968) 236–246.
[10] J. Frohly, S. Labouret, C. Bruneel, I. Looten-Baquet, R. Torguet, Ultrasonic cavitation monitoring by acoustic noise power measurement, J. Acoust. Soc. Am. 108 (5) (2000) 2012–2020.
[11] P. Bornmann, T. Hemsel, W. Sextro, T. Maeda, T. Morita, Non-perturbing cavitation detection/monitoring in sonochemical reactors, Ultrasonics Symposium (IUS), 2012, IEEE International, 2012, pp. 1141–1144 ISSN 1948–5719.
[12] P. Bornmann, T. Hemsel, W. Sextro, G. Memoli, M. Hodnett, B. Zeqiri, Self-sensing ultrasound transducer for cavitation detection, Ultrasonics Symposium (IUS), 2014, IEEE International, 2014, pp. 663–666.
[13] P. Bornmann, T. Hemsel, W. Sextro, G. Memoli, M. Hodnett, B. Zeqiri, Kavitationsdetektion mittels Self-Sensing-Ultraschallwandler, tm - Technisches Messen 82 (2) (2015) 73–84.
[14] K.A. Saalbach, J. Twiefel, J. Wallaschek, Self-sensing cavitation detection capability of horn geometries for high temperature application, J. Vibroeng. 18 (2) (2016).
[15] R. Mettin, et al., Bubble structures in acoustic cavitation: observation and modelling of a'jellyfish'-streamer, Forum Acusticum Sevilla, 2002.
[16] P. Muleki Seya, et al., Hysteresis of inertial cavitation activity induced by fluctuating bubble size distribution, Ultrason. Sonochem. 27 (2015) 262–267.
[17] J.W. Holl, A. Treaster, Cavitation hysteresis, J. Basic Eng. (1966) 199–211.
[18] P. Labelle , C. Inserra, J.-C. Bera, Cavitation level-acoustic intensity hysteresis: experimental and numerical characterization, SociétéFrançaise d'Acoustique. Acoustics 2012, Apr 2012, Nantes, France. 2012.
[19] N. Hockham, C.C. Coussios, M. Arora, A real-time controller for sustaining thermally relevant acoustic cavitation during ultrasound therapy, IEEE Trans. Ultrason. Ferroelectr. Freq. Control 57 (12) (2010).
[20] N. Hockham, M. Arora, C.C. Coussios, Closed-loop adaptive feedback control of cavitation during high-intensity focussed ultrasound therapy, J. Acoust. Soc. Am. 126 (4) (2009) 2174-2174.
[21] N. Hockham, Spatio-Temporal Control of Acoustic Cavitation During High-Intensity Focused Ultrasound Therapy (Doctoral dissertation), University of Oxford, 2013.
[22] S.R. Haqshenas, N. Saffari, Multi-resolution analysis of passive cavitation detector signals, J. Phys. Conf. Ser. 581 (1) (2015) IOP Publishing.
[23] C.-W. Lo, et al., Stabilizing in vitro ultrasound-mediated gene transfection by regulating cavitation, Ultrason. Sonochem. 21 (2014) 833–839.
[24] P. Muleki, et al., Sonoporation of adherent cells under regulated ultrasound cavitation conditions, Ultrasound Med. Biol. 41 (4) (2015) 1008–1019.
[25] J.L. Mestas, et al., Development of a confocal ultrasound device using an inertial cavitation control for transfection in-vitro, J. Phys..Conf. Ser. 656 (2015) 012003.
[26] C. Desjouy, et al., Counterbalancing the use of ultrasound contrast agents by a cavitation-regulated system, Ultrason. Sonochem. 26 (2015) 163–168.
[27] A. Sabraoui, et al., Feedback loop process to control acoustic cavitation, Ultrason. Sonochem. 18 (2011) 589–594.
[28] H. Locklar, D. Tao, L. Tarver, Automatic toner concentration control system, U.S. Patent No. 3,756,192, 4 Sep. 1973.
[29] E. Mori, S. Ueha, On the bolt-clamped Langevin type transducers, The 6th Int. Congr. on Acoustics, (1968).
[30] I. Ille, J. Twiefel, Model-based feedback control of an ultrasonic transducer for ultrasonic assisted turning using a novel digital controller, Phys. Procedia 70 (2015) 63–67.
[31] J. Twiefel, et al., Digital signal processing for an adaptive phase-locked loop controller, The 15th International Symposium on: Smart Structures and Materials & Nondestructive Evaluation and Health Monitoring, International Society for Optics and Photonics, 2008.